Journal of Solid State Chemistry 184 (2011) 3021–3027

Contents lists available at SciVerse ScienceDirect

Journal of Solid State Chemistry

journal homepage: www.elsevier.com/locate/jssc

Influence of amine-grafted multi-walled carbon nanotubes on physical and rheological properties of PMMA-based nanocomposites

Ki-Seok Kim, Soo-Jin Park*

Department of Chemistry, Inha University, Incheon 402-751, Republic of Korea

ARTICLE INFO

Article history:
Received 14 March 2011
Received in revised form
13 August 2011
Accepted 14 September 2011
Available online 17 September 2011

Keywords:
Carbon nanotubes
PMMA
Physical properties
Rheological properties

ABSTRACT

In this work, poly(methyl methacrylate) (PMMA) was grafted onto amine treated multi-walled carbon nanotubes (NH-MWNTs) and the physical and rheological properties of the NH-MWNTs–g-PMMA nanocomposites were investigated. The graft reaction of NH-MWNTs and the PMMA matrix was confirmed from the change of the N_{1S} peaks, including those of amine oxygen and amide oxygen, by X-ray photoelectron spectroscopy (XPS). The thermal and mechanical properties of the NH-MWNT–g-PMMA nanocomposites were enhanced by the graft reaction between NH-MWNTs and PMMA matrix. In addition, the viscosity of the nanocomposites was increased with the addition of NH-MWNTs. Storage (G') and loss modulus (G'') were significantly increased by increase in the NH-MWNT content compared to acid-treated MWNTs/PMMA nanocomposites. This increase was attributed to the strong interaction by the grafting reaction between NH-MWNTs and the PMMA matrix.

1. Introduction

Carbon nanotubes (CNTs) have emerged as materials of fundamental importance and great application potential due to their high aspect ratio, exceptional electrical and thermal conductivities, mechanical properties, and thermal stability [1–3]. Among various applications, CNTs have been studied as filler for polymer nanocomposites to improve thermal, mechanical, electrical, and rheological properties. Therefore, the CNTs/polymer nanocomposites are potentially valuable in semiconductors, flexible electronic systems, thin film transistors, automobiles, aerospace, etc. [4–7].

In CNTs/polymer nanocomposites, the key point is the dispersion of CNTs and interaction between polymer matrix and CNTs, because the attractive vander Waals interactions of CNTs lead to the aggregation of CNTs in the polymer matrix, resulting in the decrease of various properties of the nanocomposites. In addition, the incompatibility between polymer and smooth surface CNTs is the main factor in the defects of the nanocomposites [8–11].

Therefore, several approaches have been developed to improve the dispersion of individual CNTs in the polymer matrix, including in-situ polymerization, surface modification, ultrasonic treatment, etc. Among these, surface modification of the CNTs is one efficient approach to increase their dispersion and compatibility with polymer [12–14].

Currently, chemically non-covalent and covalent functionalization methods have been developed to modify CNTs. The chemical functionalization is the process in which functional groups are covalently linked to the CNTs' surface and the linkage is permanent and mechanically stable. However, the noncovalent functionalization linkage is not as strong as the covalent bonding formed in the chemical functionalization methods. Also, the 'grafting to' technique, which is a chemical graft reaction between functionalized CNTs and polymer, has been reported recently to enhance the dispersity and compatibility of CNTs [15–17].

In the present study, poly(methyl methacrylate) (PMMA), which is one of the most widely used thermoplastics due to its many excellent physical and optical properties, is used as the matrix. Before nanocomposite processing, multi-walled carbon nanotubes (MWNTs) were amino-functionalized using diethylene triamine (DETA). Amino functionalized MWNTs (NH-MWNTs)–g-PMMA nanocomposites were prepared by graft reaction. The effect of the NH-MWNTs on physical and rheological properties of PMMA-based nanocomposites is discussed.

2. Experimental

2.1. Materials

PMMA was obtained from LG MMA. Multi-walled carbon nanotubes (MWNTs) produced by chemical vapor deposition (CVD) process were obtained from Nanosolution Co. (Korea). The properties of the MWNTs were: purity >95 wt% and average diameter 10–25 nm. Thionyl chloride and diethylene triamine (DETA) were supplied from Aldrich. All other organic solvents used in this study were of analytical grade and used without further purification.

* Corresponding author. Fax: +82 32 860 8438.
E-mail address: sjpark@inha.ac.kr (S.-J. Park).

0022-4596/$ - see front matter © 2011 Elsevier Inc. All rights reserved.
doi:10.1016/j.jssc.2011.09.012

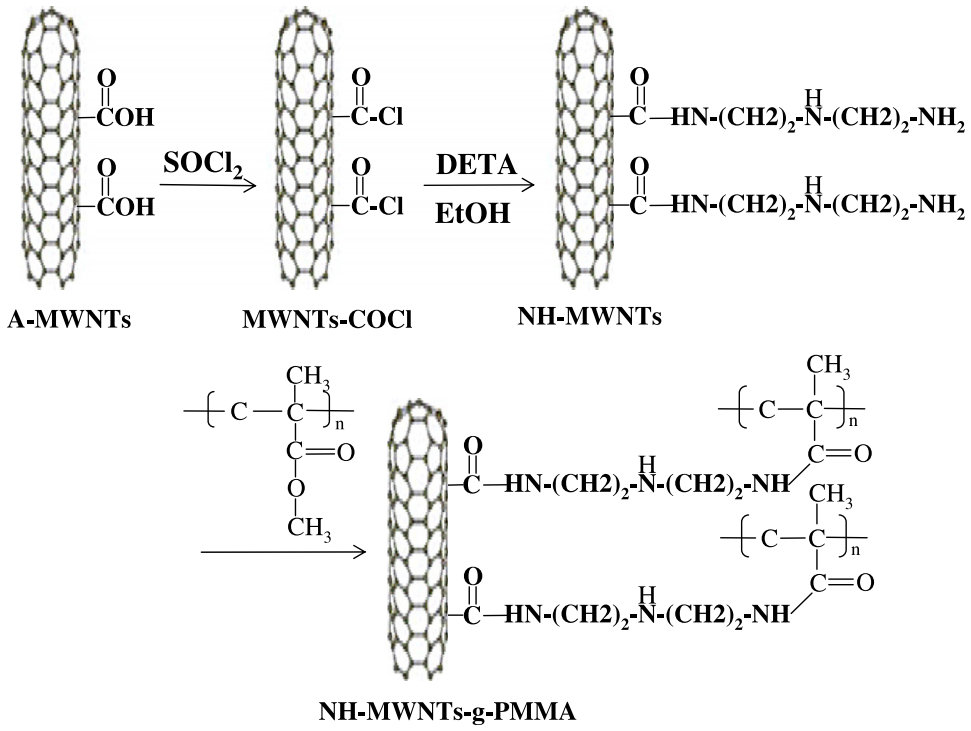

Fig. 1. Schematic diagram showing the preparation of the NH-MWNTs and NH-MWNT–g-PMMA.

2.2. Preparation of amine treated MWNTs

For the surface treatment, the MWNTs were acid-reacted with a sulfuric acid and nitric acid (3:1) mixture that was stirred for 6 h at 80 °C. They were then washed and dried at 80 °C. In the next step, the acid-treated MWNTs (A-MWNTs) were put in an excess amount of thionyl chloride and the mixture was stirred at 70 °C for 24 h. The excess thionyl chloride was decanted and the acyl-derivated MWNTs (MWNTs-COCl) were washed by THF and dried under a vacuum at room temperature. Finally, the MWNTs-COCl was reacted with excess DETA at 80 °C for 12 h and then washed by ethanol and dried at 80 °C. It was termed NH-MWNTs.

2.3. Preparation of NH-MWNT–g-PMMA nanocomposites

The NH-MWNT–g-PMMA nanocomposites were prepared with different NH-MWNT contents using a graft reaction. The NH-MWNTs concentrations were 0.5, 1, 2, and 3 wt% of the total PMMA weight. In this process, PMMA was dissolved in chloroform and NH-MWNTs were then dispersed in the PMMA solution with sonication for 3 h. Finally, the NH-MWNTs and the PMMA were reacted for 24 h at 80 °C while stirring. NH-MWNT–g-PMMA nanocomposites were prepared in a solution casting method and were then dried in an oven at 80 °C. The product was then dried in a vacuum oven at 80 °C for two days. The preparation procedure of the NH-MWNTs and NH-MWNT–g-PMMA is presented in Fig. 1.

2.4. Measurements

Structural characterization of pristine MWNTs and NH-MWNTs was determined using an FT-Raman (RFS 100S, Bruker).

Electrophoretic mobility and ζ-potential distribution of pristine MWNTs and NH-MWNTs were measured with a Zeta potential analyzer (ELS-Z, Photal otsuka).

MWNTs, NH-MWNTs, PMMA, and NH-MWNT–g-PMMA were characterized by Fourier transform infrared spectrophotometer (FT-IR 4200, Jasco) and X-ray photoelectron spectroscopy (XPS, K-Alpha) using a VG Scientific ESCALAB MK-II spectrometer equipped with an Mg$K\alpha$ (1253.6 eV) X-ray source, and a high-performance multichannel detector that was operated at 200 W.

The morphologies of the NH-MWNTs, A-MWNT/PMMA, and NH-MWNT–g-PMMA nanocomposites were observed by scanning electron microscopy (SEM, S-4200, Hitachi) and transmission electron microscope (TEM, JEM2100F, JEOL).

The electrical conductivity of the NH-MWNT–g-PMMA nanocomposites was measured at room temperature using a four-probe digital multimeter (MCP-T610, Mitsubishi Chem.).

The thermal stability of pure PMMA, A-MWNT/PMMA, and NH-MWNT-g-PMMA nanocomposites was measured by means of thermogravimetric analyses (TGA, DuPont TGA-2950 analyzer) from 30 to 850 °C at a heating rate of 10 °C/min in a nitrogen atmosphere. Number of the measurement of all samples was three times.

The mechanical properties of the A-MWNT/PMMA and NH-MWNT–g-PMMA nanocomposites were measured using the tensile strength method on a universal testing machine (UTM, Lloyd, LR5K). Each sample was tested at a crosshead speed of 2 mm/min at room temperature.

Dynamic rheological measurements of the nanocomposites were taken using an AR 1000 rheometer (TA instrument). The measurements were obtained via oscillation and steady shear tests. All measurements were performed at 230 °C. Frequency sweeps between 0.1 and 100 rad/s were carried out at low strain (5%).

3. Results and discussion

3.1. Characterization of NH-MWNTs

Fig. 2 shows the Raman spectra of pristine MWNTs and NH-MWNTs. The D peak (at 1290 cm^{-1}) and G peak (at 1590 cm^{-1}) indicate the characteristics of the MWNTs, which are attributed to the

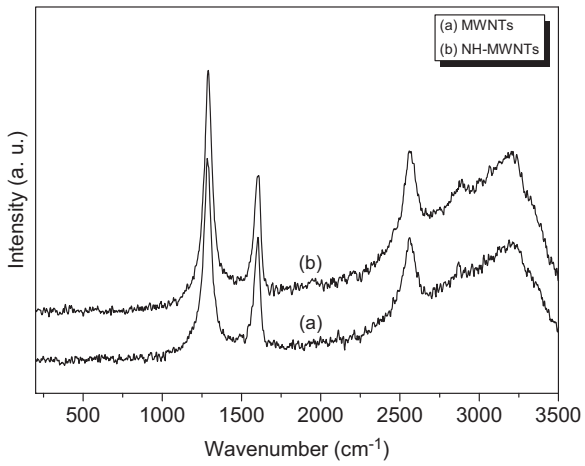

Fig. 2. Raman spectra of pristine MWNTs and NH-MWNTs.

Table 1
Zeta potential values of the A-MWNTs and NH-MWNTs.

Sample	Zeta potential (mV)	Mobility (cm^2/Vs)
A-MWNTs	−24.63	-3.25×10^{-5}
NH-MWNTs	58.18	7.67×10^{-5}

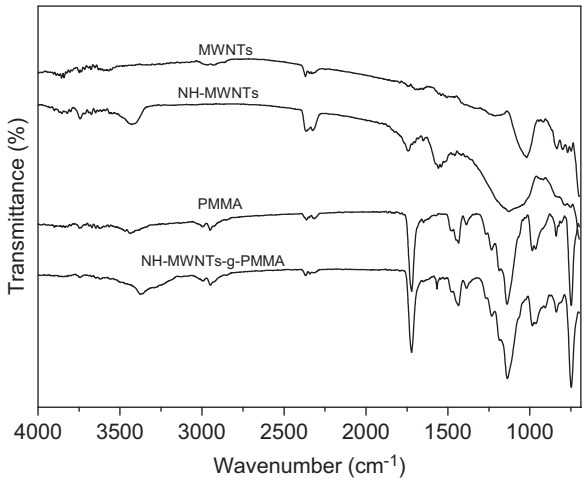

Fig. 3. FT-IR spectra of pristine MWNTs, NH-MWNTs, PMMA, and NH-MWNT–g-PMMA nanocomposites.

hexagonal framework of the MWNT wall. As shown in Fig. 2, the intensity ratio (I_D/I_G) of the *D* peak and *G* peak is weakly changed after functionalization of the MWNTs. I_D/I_G of the NH-MWNTs (1.95) increases with amine treatment of pristine MWNTs (1.75) by chemical reaction. This indicates that the acid treatment and the acylation of the MWNTs lead to the formation of sp^3 hybridized carbon defect sites and then that amine groups increase after chemical reaction with DETA [18].

Measurements of the zeta potential have long been used to study the surface chemistry of solid types. Zeta potential is calculated according to the Smoluchowski equation [19]

$$\varsigma = \frac{4\pi\eta U}{\varepsilon} \tag{1}$$

where η is the viscosity, ε the dielectric constant, and U the ion mobility; U is given by

$$U = V/E \tag{2}$$

$$\varsigma = \frac{\Lambda_V \lambda}{2n(Sin\,\theta/2)} \tag{3}$$

where E is the electric field, V the mobile velocity, n the refractive index, Λ_V the Doppler-shift, λ the wavelength, and θ the scattering angle.

The effect of surface treatment using DETA on the electrophoretic characteristics of the carbon nanotube dispersants in ethanol is determined using zeta potential measurements; the values are shown in Table 1.

Zeta potential value and electrophoretic mobility of the NH-MWNTs are increased with chemical surface treatment compared with pristine MWNTs, indicating fairly stable dispersion of NH-MWNTs relative to pristine MWNTs in ethanol. This stable dispersion is attributed to the formation of an electrical double layer that is an ionic volume of a few angstrom thicknesses that

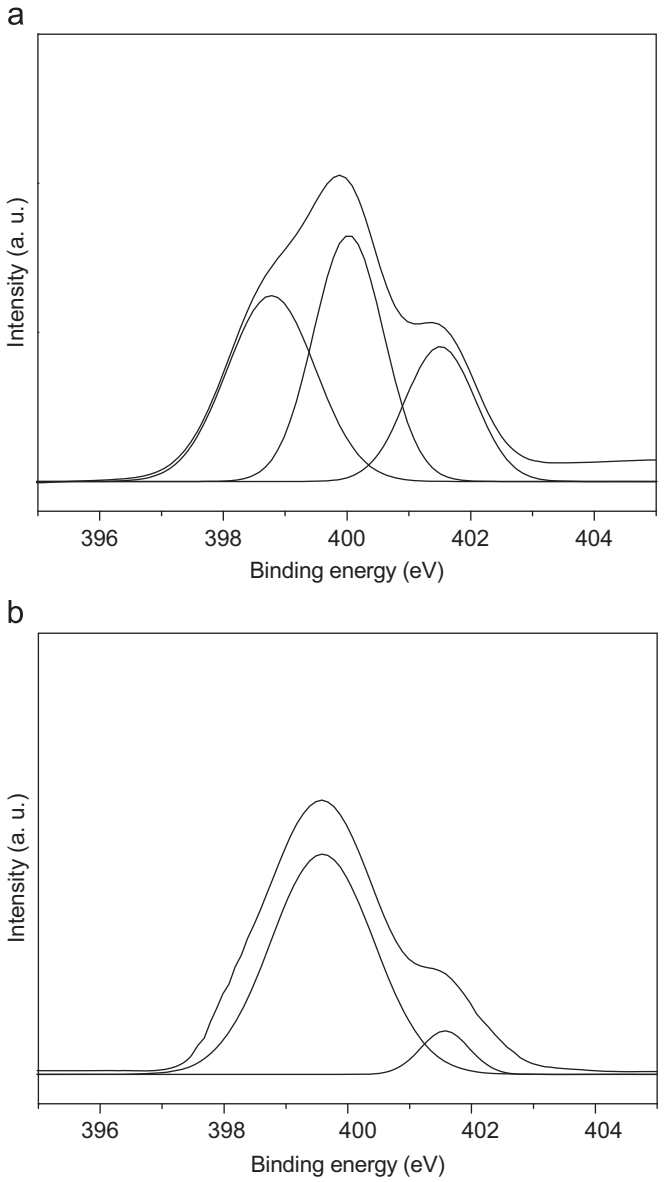

Fig. 4. XPS N_{1S} spectra of (a) NH-MWNTs and (b) NH-MWNT–g-PMMA nanocomposites.

prevents the particle aggregation and thereby stabilizes the suspension. In the present case, the dissociation of amine groups increased by chemical treatment in the presence of ethanol leads to the formation of the electrical double layer around the particles, preventing the aggregation and resulting in the increase of the zeta potential value [20,21].

3.2. Grafting of PMMA onto NH-MWNTs

Fig. 3 shows the FT-IR spectra of pristine MWNTs, NH-MWNTs, PMMA, and NH-MWNT–g-PMMA nanocomposites. There are no characteristics of pristine MWNTs. In NH-MWNTs, the appearance of a weak and broad band at 3400 cm^{-1}, carbonyl stretching at 1720 cm^{-1}, and absorbance at 1560 cm^{-1} are, respectively, attributed to hydroxyl groups, carbonyl groups, and amino groups on the surface of the NH-MWNTs, resulting from the functionalization of the MWNTs. The PMMA and NH-MWNT–g-PMMA nanocomposites show a strong carbonyl peak at 1730 cm^{-1} and NH-MWNT–g-PMMA nanocomposites exhibit amino groups at 1560 cm^{-1}, like NH-MWNTs. It indicates that PMMA is grafted onto the NH-MWNTs [22].

The grafting of PMMA onto the NH-MWNTs is confirmed by XPS analysis, as shown in Fig. 4. The N_{1S} peak of the NH-MWNTs can be curve-fitted with three component peaks, as shown in Fig. 4(a). The lower binding energy peak at 398.7 eV is attributed to the amine nitrogen. The higher binding energy peaks at 400.0 and 401.5 eV are attributed to the amide nitrogen by the electron-withdrawing carbonyl group. Fig. 4(b) shows the N_{1S} spectrum of the NH-MWNT–g-PMMA nanocomposites after the graft reaction. The N_{1S} peak can also be curve-fitted with two component peaks, one at 400.0 eV and the other at 401.5 eV. The absence of an amine nitrogen peak at 398.7 eV reveals that all the amine groups of the NH-MWNTs have reacted with the PMMA.

3.3. Electrical properties of the nanocomposites

The microstructure of NH-MWNTs and NH-MWNT–g-PMMA nanocomposites is confirmed using SEM, and is shown in Fig. 5. It can be seen that the NH-MWNTs exhibit diameters in the range of about 20–60 nm and length of a few micrometers. Also, they are entangled and randomly oriented. After nanocomposite processing, NH-MWNTs are uniformly dispersed in the PMMA matrix without aggregation, which is attributed to the strongly interfacial interaction between NH-MWNTs and PMMA throughout graft reaction. The dispersion of A-MWNTs and NH-MWNTs in the PMMA matrix is further observed using TEM images, as shown in Fig. 5(c) and (d). In A-MWNT/PMMA, A-MWNTs display localized aggregation, whereas the NH-MWNTs is highly dispersed in PMMA without aggregation between MWNTs. It is indicated that the more effective surface modification of MWNTs lead to the decrease of a size of the clusters with less entangled MWNTs, resulting from the decrease of strong π–π interaction between individual MWNTs and the increase of the interaction between NH-MWNTs and PMMA matrix. Moreover, NH-MWNTs dispersed in the PMMA matrix form an interconnected network, resulting in an electrical conductive pathway in nanocomposite system [9].

Measurement of electrical conductivity is important to qualify the conductive polymer composites, and is influenced by filler content, filler type, and dispersion of filler. In this work, to improve the dispersity of MWNTs and interaction between MWNTs and polymer matrix, the chemically functionalized MWNTs using DETA are used.

Electrical conductivity of the PMMA nanocomposites as a function of NH-MWNT content is listed in Table 2. The electrical conductivity of neat PMMA is not detectable (over the limit of equipments). The electrical conductivity of the nanocomposites is

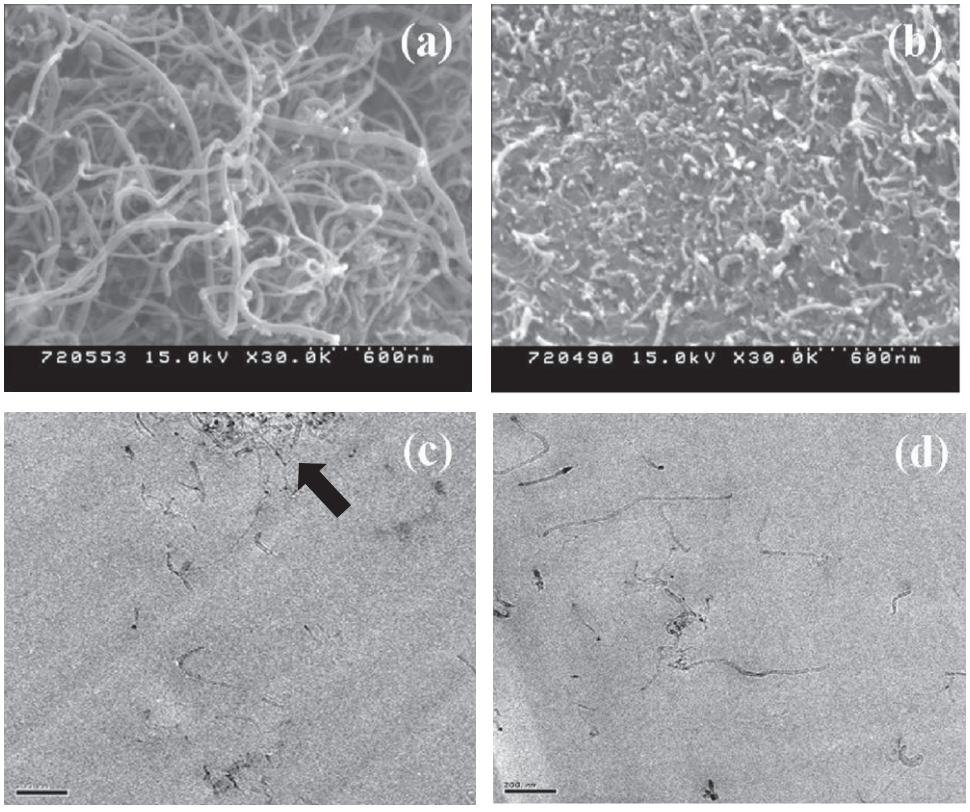

Fig. 5. SEM images of (a) pristine MWNTs, (b) NH-MWNT–g-PMMA nanocomposites, and TEM images of (c) A-MWNTs/PMMA and (d) NH-MWNT–g-PMMA nanocomposites.

Table 2
Electrical conductivity of the nanocomposites as a function of MWNT content.

MWNTs (wt%)	A-MWNTs/PMMA (Ω cm)	NH-MWNTs–g-PMMA (Ω cm)
0.5	–	9.3×10^5
1	4.0×10^4	4.9×10^4
2	4.1×10^3	1.4×10^4
3	1.6×10^3	2.5×10^3

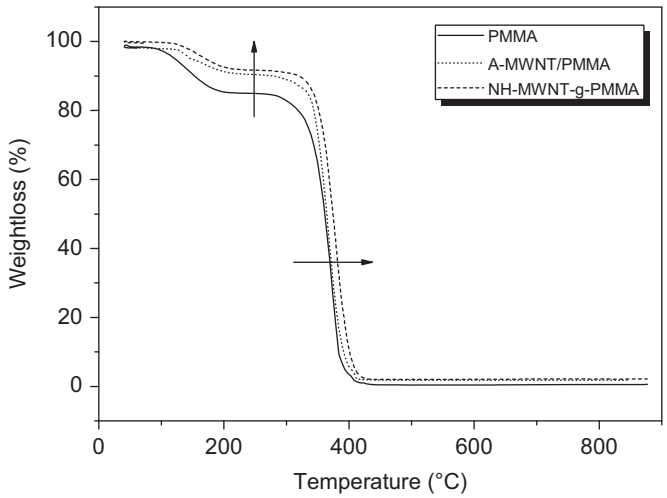

Fig. 6. TGA thermogram of neat PMMA, A-MWNT/PMMA, and NH-MWNT–g-PMMA nanocomposites ($n=3$).

steadily increased with increase in MWNT content. It is noted that MWNTs are homogeneously dispersed in the PMMA matrix and form an interconnected MWNT network, resulting in the formation of a conductive network. Also, the densely conductive network is formed with the increase of MWNT content, leading to the increase of the electron pathway. However, the electrical conductivity of the NH-MWNT–g-PMMA is lower than that of A-MWNT/PMMA over 0.5 wt% MWNTs due to the higher dispersity and shorter length and aspect ratio of NH-MWNTs after chemical functionalization [23].

3.4. Physical properties of the nanocomposites

The thermal stabilities of pure PMMA, A-MWNTs/PMMA, and NH-MWNTs–g-PMMA are shown in Fig. 6. The initial decomposed temperature (IDT) of the A-MWNT/PMMA (166 °C) and NH-MWNT–g-PMMA nanocomposites (171 °C) is higher than that of the pure PMMA (126 °C). The NH-MWNT–g-PMMA nanocomposites become degraded near 373 °C, which is a higher temperature compared to the degradation temperature of pure PMMA (359 °C) and A-MWNT/PMMA (363 °C). This is attributed to the grafting between the NH-MWNTs and PMMA, which causes a trammel effect of the movement of the PMMA chains. In addition, no significant weight change was observed at temperatures in excess of approximately 430 °C; moreover, the residual weight percent of the nanocomposites is higher (1.8–2.1%) than that of the pure PMMA (0.6%). These results indicate that the difference in the total weight loss is most likely due to the excellent thermal stability of the NH-MWNTs dispersed in the PMMA matrix [24].

Fig. 7 shows the tensile strength and modulus of the PMMA nanocomposites as a function of MWNT content. The tensile strength of the nanocomposites is improved by increasing the MWNT content. The maximum value of the tensile strength is shown in 1.0 wt% A-MWNTs and NH-MWNT loading and is higher

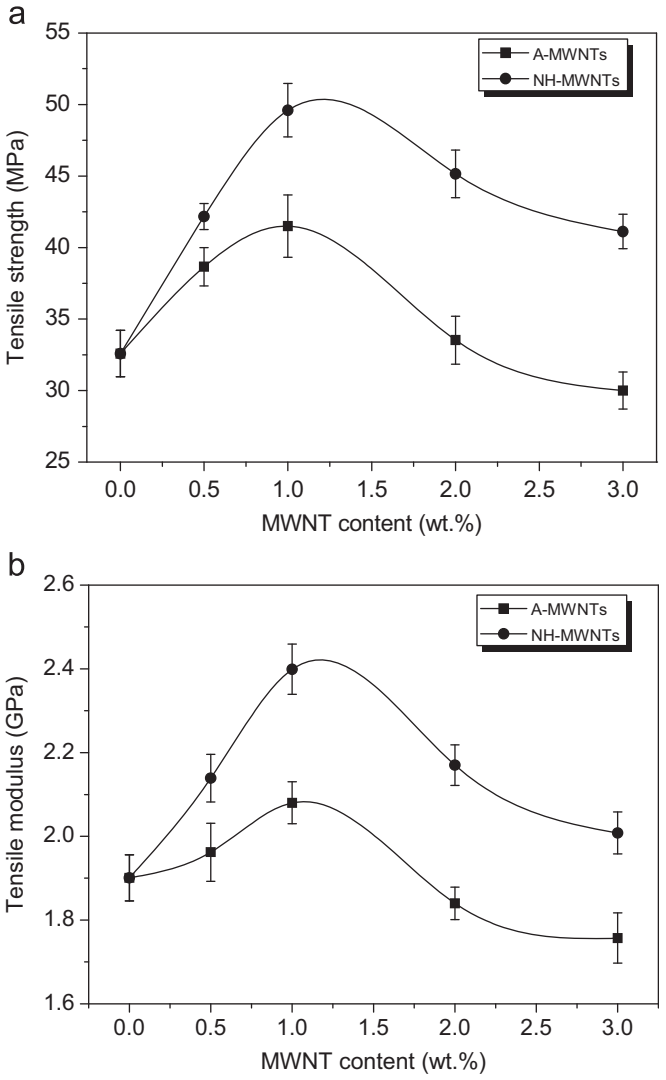

Fig. 7. Tensile strength and modulus of A-MWNT/PMMA and NH-MWNT–g-PMMA nanocomposites with different MWNT contents.

by about 29% and 50%, respectively, than that of pure PMMA. Likewise, the maximum tensile modulus values are obtained with 1.0 wt% A-MWNTs and NH-MWNT loading, and is about 9% and 26% greater than that of pure PMMA, respectively. It is clear that although the physical properties of A-MWNT/PMMA are higher than that of pure PMMA by highly dispersed A-MWNTs in PMMA matrix, NH-MWNTs are more effective reinforcement for the PMMA nanocomposites, resulting from strong intermolecular interaction via the grafting between NH-MWNTs and the PMMA matrix (see Fig. 1). Above 1.0 wt% MWNTs, the mechanical properties of the nanocomposites are slightly decreased due to the accumulation of MWNTs. However, the decrease of the tensile strength of NH-MWNT–g-PMMA nanocomposites is lower than that of A-MWNT/PMMA for over 1.0 wt% MWNTs. It is suggested that the chemical functionalization of the MWNTs causes a higher dispersity in the PMMA matrix, resulting in enhanced interfacial bonding between MWNTs and the PMMA matrix [25].

3.5. Rheological properties of the nanocomposites

Fig. 8 shows the viscosity obtained for the NH-MWNT–g-PMMA nanocomposites containing different contents of NH-MWNTs at different frequencies. Fig. 8 shows that the NH-MWNT-reinforced nanocomposites display higher viscosity compared to pure PMMA

and the viscosity of the PMMA increases as the NH-MWNT content increases. The addition of a low content of MWNTs (0.5 wt%) induces a small increase in the viscosity. This behavior is similar to that of PMMA, though PMMA containing relatively high content of MWNTs (1.0–3.0 wt%) shows increased viscosity at low frequency, which then gradually decreases as the frequency increases. This indicates that the increase of the viscosity is mainly related to the formation of an interconnected structure of the MWNTs and an increase in the NH-MWNT content leads to an increase in shear thinning behaviors. Also, the network of the MWNTs leads to restraining the motion of the polymer chains [26].

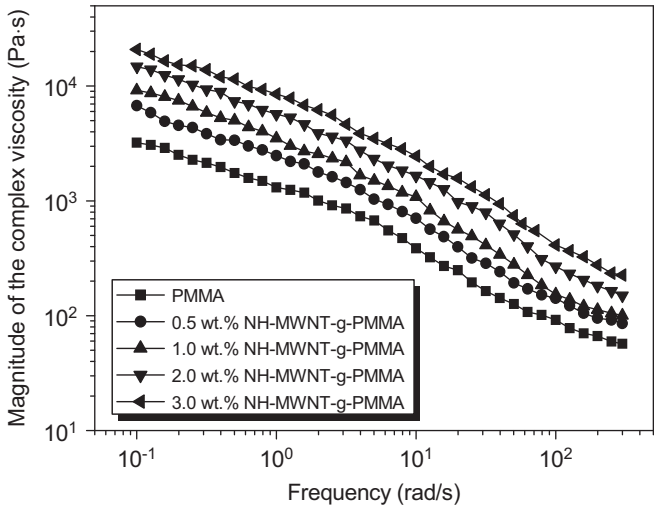

Fig. 8. Complex viscosity of NH-MWNT–g-PMMA nanocomposites with different NH-MWNT contents.

Fig. 9 shows the storage modulus (G') and loss modulus (G'') of the A-MWNTs/PMMA and NH-MWNTs–g-PMMA nanocomposites with different MWNT contents. As well known, in carbon nanotube-reinforced polymer nanocomposites, the surface modification of the carbon nanotubes is significantly affected due to the physical and rheological properties of the polymer, resulting from the strong physical interaction or chemical reaction between carbon nanotubes and polymer matrix. In our previous study [27], we have confirmed that glycidyl methacrylate-grafted MWNTs provides higher physical and rheological properties of PMMA-based nanocomposites compared to conventional acid-treated MWNTs, indicating that surface modified carbon nanotubes are resulted in the improved compatibility between carbon nanotubes and polymer, leading to good dispersion of carbon nanotubes in polymer matrix.

In Fig. 9, the G' value of NH-MWNTs–g-PMMA is higher than that of A-MWNTs/PMMA, indicating the difference of dispersion

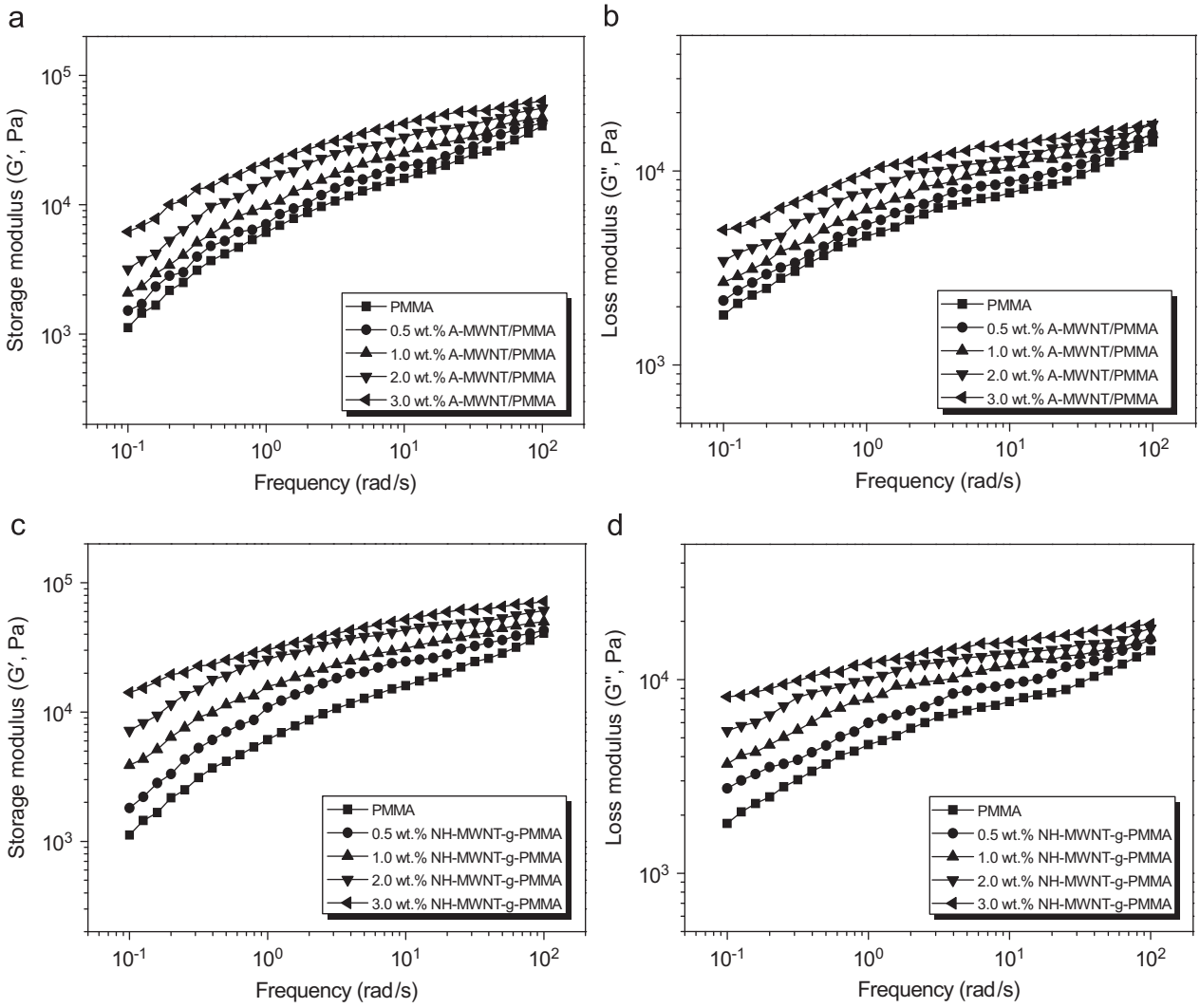

Fig. 9. Storage modulus G' and loss modulus G'' of (a, b) A-MWNT/PMMA and (c, d) NH-MWNT–g-PMMA nanocomposites with different MWNT contents.

of MWNTs and interaction between MWNTs and PMMA. Compared to conventional acid-treated MWNTs, amine treated MWNTs can provide improved dispersion, leading to the formation of the CNT's network at relative low MWNT content and strong interaction between MWNTs and polymer matrix by grafting reaction, as mentioned from thermal and mechanical properties as well as rheological property. Du et al. [28] have reported the effect of degree of dispersion of SWCNTs on rheological properties of SWNTs/PMMA. They indicated that higher G' values are significantly related to the dispersion of SWNTs. In addition, both the G' and G'' values of the nanocomposites increase monotonically for all frequencies, representing more solid-like behavior as the MWNT content increases.

In carbon nanotube reinforced composite system, rheological behaviors at low frequency is useful to examine the change of micro- and nano-stucture of CNTs-filled polymer composites and 'pseudo-solid like' properties. As shown in Fig. 9c and d, at low frequencies, G' and G'' are significantly increased with increase in NH-MWNT content and the effect of the NH-MWNT content on G' and G'' is much higher at a low frequency than at a high frequency, indicating the transition from liquid-like to solid-like by the formation of MWNT network in the composites. Moreover, the increase in G' as a function of the NH-MWNT content is larger than that of G''. This difference indicates that the structure of the nanocomposites is sensitively reflected on G'. Consequently, the rheological properties of the nanocomposites are enhanced with the addition of NH-MWNTs. This enhancement is attributed to chemical reaction between the NH-MWNTs and PMMA during nanocomposite processing [29].

4. Conclusion

Amine-treated MWNT-g-PMMA nanocomposites were prepared by graft reaction. The grafting of PMMA onto the NH-MWNTs was confirmed by means of XPS, showing that it resulted from the shift of the N_{1S} peaks. The electrical conductivity of the NH-MWNT–g-PMMA nanocomposites increased as the NH-MWNT content increased due to the increase in the number of electron conductive pathways. The thermal and mechanical properties of the NH-MWNT–g-PMMA nanocomposites were improved with the addition of NH-MWNTs. It was found that the grafting of NH-MWNTs and the PMMA matrix led to an effective reinforcement effect for the nanocomposites. Additionally, rheological properties were remarkably increased by increase in the NH-MWNT content, which increase was attributed to the strong interaction between NH-MWNTs and PMMA by graft reaction.

Acknowledgment

This work was supported by Carbon Valley Development Project of the Ministry of Knowledge Economy, Korea.

References

[1] E.N. Konyushenko, J. Stejskal, M. Techova, J. Hradil, J. Kovarova, J. Prokes, M. Cieslar, J.Y. Hwang, K.H. Chen, I. Sapurina, Polymer 47 (2006) 5715–5723.
[2] S. Stehlik, J. Orava, T. Kohoutek, T. Wagner, M. Frumar, V. Zima, T. Hara, Y. Matsui, K. Ueda, M. Pumera, J. Solid State Chem. 183 (2010) 144–149.
[3] P. Chen, H.S. Kim, H.J. Jin, Macromol. Res. 17 (2009) 207–217.
[4] Q.H. Zhang, S. Rastogi, D.J. Chen, D. Lippits, P.J. Lemstra, Carbon 44 (2006) 778–785.
[5] J. Wang, M. Musameh, Y. Lin, J. Am. Chem. Soc. 125 (2003) 2408–2409.
[6] A. Nojeh, G.W. Lakatos, S. Peng, K. Cho, R.F.W. Pease, Nano Lett. 3 (2003) 1187–1190.
[7] G. Zheming, L. Chunzhong, W. Gengchao, Z. Ling, C. Qilin, L. Xiaohui, W. Wendong, J. Ind. Eng. Chem. 16 (2010) 10–14.
[8] M.A.L. Manchado, L. Valentini, J. Biagiotti, J.M. Kenny, Carbon 43 (2005) 1499–1505.
[9] B.K. Zhu, S.H. Xie, Z.K. Xu, Y.Y. Xu, Comps. Sci. Technol. 66 (2006) 548–554.
[10] E.V. Basiuk, T.Y. Gromovoy, A. Datsyuk, B.B. Palyanytsya, V.A. Pokrovskiy, V.A. Basiuk, J. Nanosci. Nanotechnol. 5 (2005) 984–990.
[11] J.T. Han, J.S. Woo, H.J. Jeong, S.Y. Jeong, G.W. Lee, Carbon Lett. 12 (2011) 90–94.
[12] A. Star, Y. Liu, K. Grant, L. Ridvan, J.F. Stoddart, D.W. Steuerman, M.R. Diehl, A. Boukai, J.R. Heath, Macromolecules 36 (2003) 553–560.
[13] S.J. Park, M.S. Cho, S.T. Lim, H.J. Choi, M.S. Jhon, Macromol. Rapid. Commum. 24 (2003) 1070–1073.
[14] B.X. Yang, J.H. Shi, K.P. Pramoda, S.H. Goh, Comp. Sci. Tech. 68 (2008) 2490–2497.
[15] M.J. Sobkowicz, J.R. Dorgan, K.W. Gneshin, A.M. Herring, J.T. McKinnon, Carbon 47 (2009) 622–628.
[16] T. Ramanathan, H. Liu, L.C. Brinson, J. Polym. Sci. B: Polym. Phys. 43 (2005) 2269–2279.
[17] C. Gao, Y.Z. Jin, H. Kong, R.L.D. Whitby, S.F.A. Acquah, G.Y. Chen, H.H. Qian, A. Hartschuh, S.R.P. Silva, S. Henley, P. Fearon, H.W. Kroto, D.R.M. Walton, J. Phys. Chem. B 109 (2005) 11925–11932.
[18] G.M. Yang, C.C. Yang, Q. Xuc, W.T. Zheng, S. Li, J. Solid State Chem. 182 (2009) 3393–3398.
[19] S.J. Park, J.S. Kim, Carbon 39 (2001) 2011–2016.
[20] H. Hu, A. Yu, E. Kim, B. Zhao, M.E. Itkis, E. Bekyarova, R.C. Haddon, J. Phys. Chem. B 109 (2005) 11520–11524.
[21] A.R. Boccaccini, J. Cho, J.A. Roether, B.J.C. Thomas, E.J. Minay, M.S.P. Shaffer, Carbon 44 (2006) 3149–3160.
[22] M. Coskun, K. Demirelli, Polym. Degrad. Stab. 51 (1996) 173–178.
[23] C.A. Martin, J.K.W. Sandler, M.S.P. Shaffer, M.K. Schwarz, W. Bauhofer, K. Schulte, A.H. Windle, Comp. Sci. Technol. 64 (2004) 2309–2316.
[24] M. Xiao, Y. Lu, S.J. Wang, Y.F. Zhao, Y.Z. Meng, J. Power Sources 160 (2006) 165–174.
[25] M.K. Seo, J.R. Lee, S.J. Park, Mater. Sci. Eng. A 404 (2005) 79–84.
[26] E. Franchini, J. Galy, J.F. Gérard, J. Colloid Interf. Sci. 329 (2009) 38–47.
[27] K.S. Kim, J.H. Byun, G.H. Lee, S.J. Park, Macromol. Res. 19 (2011) 14–20.
[28] F. Du, R.C. Scogna, W. Zhou, S. Brand, J.E. Fischer, K.I. Winey, Macromolecules 37 (2004) 9048.
[29] H.J. Choi, J.Y. Lim, K. Zhang, Diamond Relate. Mater. 17 (2008) 1498–1501.